International Nano Letters
a SpringerOpen Journal

ORIGINAL ARTICLE Open Access

Defect generation, *d-d* transition, and band gap reduction in Cu-doped TiO_2 nanoparticles

Biswajit Choudhury*, Munmun Dey and Amarjyoti Choudhury

Abstract

TiO_2 doped with Cu^{2+} initiates the formation of brookite phase along with anatase. Doping of Cu^{2+} introduces structural defects into TiO_2. The direct evidence is the low intense and broad diffraction peaks. Raman peaks of doped TiO_2 are also broad and are blueshifted. Pure TiO_2 exhibits an absorption in the UV region, the position of which is shifted towards the visible region on incorporation of Cu into it. The visible absorption peaks arise due to the *d-d* transition of Cu^{2+} in the crystalline environment of TiO_2. Incorporation of Cu^{2+} distorts the local structure of TiO_2, resulting in the loss of octahedral symmetry surrounding Cu^{2+}. The Jahn-Teller distortion splits the ^2E_g and $^2T_{2g}$ state of Cu^{2+} into several *d* states. Interaction of light excites the electron from ground to several of the excited states and gives the visible absorption peaks in the framework of TiO_2. These Cu^{2+} *d* states and oxygen defects create band states, thereby favoring electronic transition to these levels and resulting in lowering of band gap of TiO_2. A direct confirmation is the increase in the magnitude of Urbach energy with the reduction in the band gap of doped TiO_2.

Keywords: Defects, Raman peak, Blueshift, Crystal field, Band gap

Background

TiO_2 is an important transition metal oxide material with a major application area in photocatalysis, where it shows its efficiency in the removal of unwanted impurities from water, air, etc. [1,2]. The main drawback of pure TiO_2 is its wide band gap (3 to 3.2 eV); because of which, it absorbs only the UV part of solar radiation that accounts for only 4% of the total solar radiation, leaving most of the visible portion of light [2,3]. This material can be made visible light-active either by introducing structural defects such as Ti^{3+} and oxygen vacancies or by incorporation of non-metals such as N, C, and S, and transition and rare earth ions [3-10]. These defects and dopants create sub-band states in the band gap of TiO_2 and shift the absorption edge of TiO_2 towards the visible region, thus enhancing the visible light photoactivity. Structural defects, generated on doping, can effectively tune the band structure and control the photoactivity. In Fe, Ce-codoped TiO_2, it is reported that doping of these ions leads to the creation of grain boundary defects and results in the bending of the valence and conduction bands. These defects limit the electron mobility to the interface and prevent charge carrier recombination [11]. Cu is also an important dopant because it has high electronic conductivity, and it is cheap and highly available on the Earth's crust [12]. Cu-doped TiO_2 or CuO/TiO_2 composite serves as an efficient photocatalytic material in the decomposition of gas-phase alcohols, acid orange 88, methylene blue, etc. [13-15]. Cu doping can effectively reduce the wide band gap of TiO_2 by creating defects and *d*-band states of Cu in TiO_2 and can also act as active trap centers of electrons to reduce carrier recombination [3,16]. Other applications of Cu-doped TiO_2 are as anode materials in Li-ion batteries [12], CO sensing [17], NO and CO_2 reduction [18,19], etc. Cu-doped TiO_2 also shows activity in bacterial inactivation [20]. In this article, we have discussed the doping effect of Cu on the crystallinity of pure TiO_2 nanoparticles. We have examined how Cu extends the absorption edge of TiO_2 to the visible region and reduces the effective band gap of TiO_2. The structural characterizations are done with X-ray diffraction, transmission electron microscopy, and Raman spectroscopy, while absorption spectra are analyzed in a UV–vis spectrometer in diffuse reflectance mode.

Methods

TiO_2 nanoparticles with 2%, 4%, and 6% Cu were prepared by sol–gel method. The synthesis started with the addition of 10 ml of titanium isopropoxide (Sigma-Aldrich

* Correspondence: biswajit@tezu.ernet.in
Department of Physics, Tezpur University, Napaam, Assam 784028, India

Corporation, St. Louis, MO, USA) to a mixture of 20 ml 2-propanol (Merck, Worli, Mumbai, India) and 10 ml of ethanol (Merck). The reaction mixture was stirred for 15 min, and then 1 ml of water was added to hydrolyze the isopropoxide chain. This was followed by dropwise addition of copper nitrate hexahydrate (Merck) solution with the requisite amount of Cu. The solution was stirred for 6 h, and after this time, the solution was transformed to gel. The gel was centrifuged in water and ethanol for five times and then dried in a vacuum oven at 80°C to get an amorphous Cu-doped TiO_2 nanopowder. The nanopowder was then annealed in air at 450°C for 4 h to obtain Cu-doped TiO_2 nanoparticles.

The X-ray diffraction (XRD) pattern of the samples was characterized using a Rigaku MiniFlex X-ray diffractometer (Rigaku, Tokyo, Japan) with CuKα radiation (λ = 1.54 Å) at a scanning angle between 20° and 70°. The high-resolution transmission electron microscope (TEM) images of the doped nanoparticles are obtained using a JEOL-JEM-2100 transmission electron microscope (JEOL Ltd., Tokyo, Japan) at an operating voltage of 200 kV. Energy dispersive X-ray (EDX) spectra of the samples were studied with a JEOL JSM (model 6390 LV) scanning electron microscope with an INCAx-Sight EDX detector (Oxford Instruments, Abingdon, Oxfordshire, UK). The Raman spectra of the samples were recorded using a Renishaw In-Via Raman spectrometer (Renishaw, Wotton-under-Edge, UK) at a resolution of 0.3 cm^{-1}. Electron paramagnetic resonance (EPR) spectra were obtained using a Bruker EMX 300 EPR spectrometer (Bruker BioSpin GmbH, Silberstreifen 4, Germany), Diffuse reflectance spectra (DRS) of the samples were obtained using a Shimadzu 2450 UV–vis spectrophotometer (Shimadzu Corporation, Kyoto, Japan) with $BaSO_4$ powder as the standard reference sample.

Results and discussion

X-ray diffraction analysis

The diffraction pattern of pristine and Cu-doped TiO_2 nanoparticles is shown in Figure 1. The diffraction pattern corresponds to the tetragonal anatase phase of TiO_2 (JCPDS-782486). Indeed, a small fraction of brookite phase is also present in between 27° and 36°, and at 40° (JCPDS-761934). Anatase and brookite are the metastable phases of TiO_2 and usually formed at low temperature during solution-phase synthesis. Presence of brookite phase has also been observed by So et al. in TiO_2 nanoparticles [21]. They reported that the brookite phase completely disappeared at high annealing temperature. Increase in the brookite fraction with doping indicates inhibition of the formation of complete anatase phase due to incorporation of Cu on the lattice site or grain boundary. The crystallite size of the samples is calculated by using

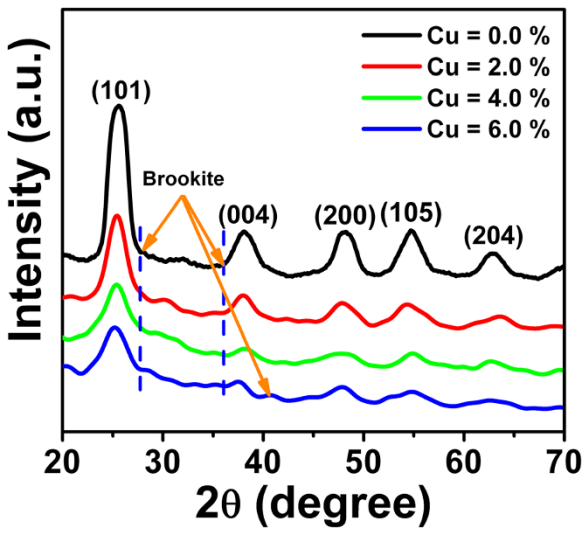

Figure 1 XRD pattern of pure and Cu-doped TiO_2 nanoparticles with 2%, 4%, and 6% of Cu loading.

Scherrer's equation, $d = \frac{0.9\lambda}{\beta \mathrm{Cos}\theta}$, where d is the crystallite size, λ is the wavelength of X-ray radiation, β is full width at half maximum, and θ is the diffraction angle. The resultant sizes are 6, 5.5, 5, and 4 nm for pristine and 2%, 4%, and 6% Cu, respectively. The diffraction peaks are broad in all the samples. The widening of the XRD peaks indicates reduction in the grain size and increase in the fraction of the amorphous grain boundary, containing many of the structural defects. The diffraction peak intensity is lower in the doped samples than in the pristine one. The low intense diffraction peaks indicate degradation of structural quality or loss of crystallinity of TiO_2 on doping.

TEM and EDX analysis

The high-resolution transmission electron microscope images of 2%, 4%, and 6% Cu-doped TiO_2 nanoparticles are shown in Figure 2a,b,c. The particles are spherical in shape with some amount of agglomeration. The particle size distribution shows that the average numbers of particles have a size of 9, 8, and 8 nm, respectively, for 2%, 4%, and 6% Cu-doped TiO_2. Therefore, doping does not affect the size of the nanoparticles. Figure 2d,e,f shows the EDX pattern of the 2%, 4%, and 6% Cu-doped TiO_2 nanoparticles, showing the presence of Cu, Ti, and oxygen in the nanoparticles. There is no peak of nitrogen in the EDX, indicating removal of nitrate impurities during centrifugation.

Raman spectroscopy study

Raman spectroscopy is a technique of importance for the understanding of the local structure changes on incorporation of dopant ions. The Raman spectra of our samples are shown in Figure 3.

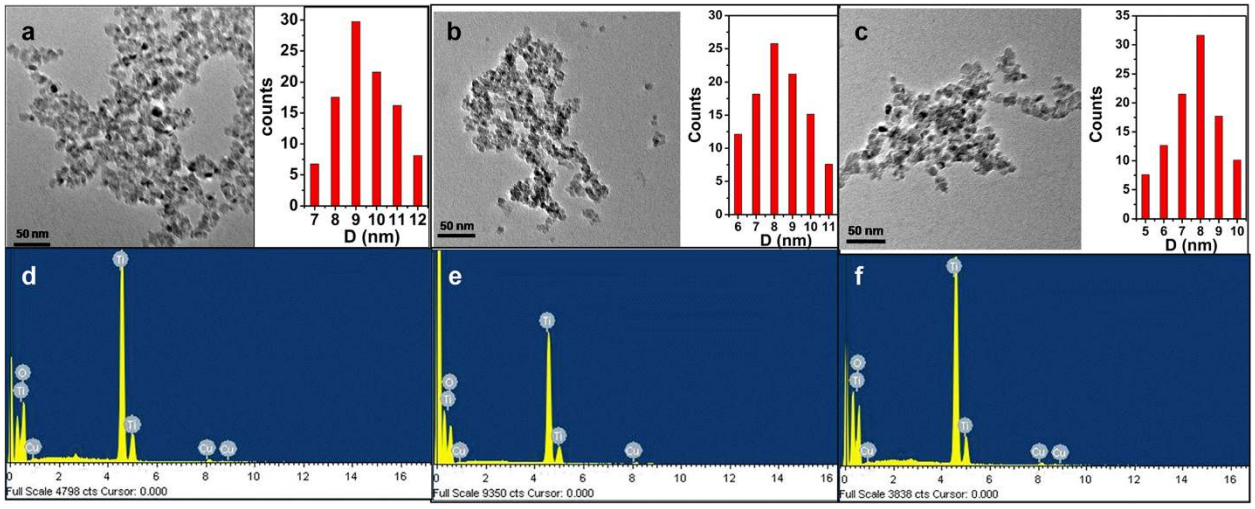

Figure 2 TEM images. (**a**) 2%, (**b**) 4%, and (**c**) 6% Cu-doped TiO_2nanoparticles. (**d**, **e**, **f**) The EDX pattern of the 2%, 4%, and 6% Cu-doped TiO_2.

The Raman spectra of our samples correspond to the anatase phase of TiO_2. We have not detected any secondary peaks related to Cu or its oxide phases. The intense peak at 149 cm^{-1} corresponds to the E_g mode of anatase TiO_2 [22,23]. Other than this, two other low intense modes appear at 197 and 641 cm^{-1}, respectively. The B_{1g} mode occurs at 400 cm^{-1}, and the A_{1g} + B_{1g} mode appears at 530 cm^{-1}, respectively [23]. The significant observation in the Raman peaks of the samples is the broadness and shifting to a higher wavenumber with Cu loading. Any characteristic Raman vibration is associated with the Ti-O stretching, bending vibration [24]. The E_g peak is associated with the symmetric stretching vibration of O-Ti-O in TiO_2, the B_{1g} peak is due to the symmetric bending vibration of O-Ti-O, and the A_{1g} peak is the result of antisymmetric bending vibration of O-Ti-O [24]. The ionic size of Cu^{2+} (0.73 Å) is larger than that of Ti^{4+} (0.64 Å), and hence, doping of this ion will distort the lattice structure of TiO_2; since there is charge difference between Cu^{2+} and Ti^{4+}, doping of Cu generates oxygen vacancies in the lattice of TiO_2 to maintain the charge neutrality [3]. If doping occurs on the substitutional position on the Ti^{4+} site, the Ti-O-Ti bond will be disturbed and a new Cu-O-Ti or Cu-O-Cu bond will be formed. Therefore, disturbance of the Ti-O-Ti bonds and the formation of new Cu-O bonds will affect the Raman-active modes and will result in the broadening and shifting of the peaks. Although Cu^{2+} doping on the Ti^{4+} site will affect the entire Raman-active modes, we have considered the intense E_g peak to understand the doping effect. The E_g peak is associated with the Cu-O-Cu stretching mode vibration, and on doping, the strength of this vibration lowers, since oxygen vacancy is formed nearby. The formation of oxygen vacancy nearby Cu is theoretically proved in the Cu-doped TiO_2 system [25]. Due to the generation of these oxygen vacancies, the lattice is contracted and the peak is shifted to a higher wavenumber. Perker and Siegel in their work reported that oxygen vacancies are responsible for the shifting and broadening of the Raman peak [26]. On the other hand, some people reported that quantum size effect has a role to play in the broadening and peak shifting [27]. From XRD and TEM, we have found that the size of the nanoparticles is in the nanoregime; therefore, phonon confinement will be prominent. Alongside, XRD also demonstrates that grain boundary defects are also generated. Therefore, both phonon confinement and structural defects may result in the shifting and broadening of the Raman E_g peak. The oxygen vacancy generation

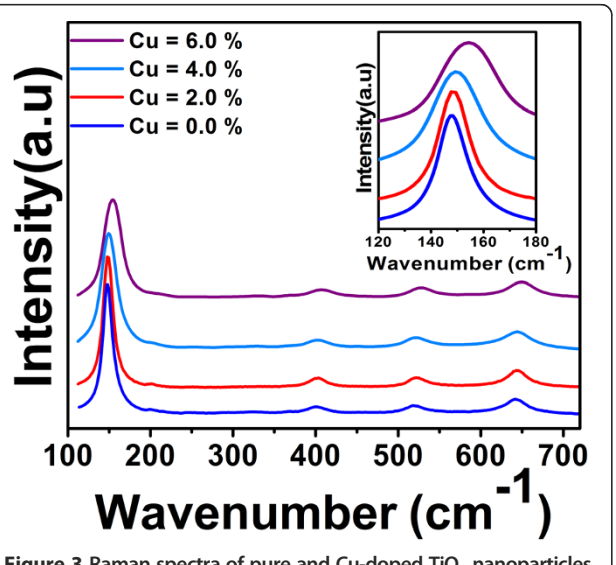

Figure 3 Raman spectra of pure and Cu-doped TiO_2 nanoparticles. The inset of the figure shows the enlarged view of the E_g mode of the nanoparticles.

and lattice disruption of Cu-doped TiO_2 are shown in Figure 4a.

Electron paramagnetic resonance spectra analysis

Electron paramagnetic resonance (EPR) is an important tool to understand the valence state of the dopant and the coordination environment of the dopant in the framework of the host. The EPR spectra of 2% Cu-doped TiO_2 nanoparticles are shown in Figure 5. As shown in the spectra, the EPR spectra are asymmetric in shape and contain a signal corresponding to the presence of Cu^{2+} in the distorted octahedral coordination of TiO_2 [15,28]. The intense peak is centered at $g_\perp$ = 2.08 followed by less intense quadruple signals at g_{II} = 2.21, 2.28, 2.38, and 2.48, respectively, in the lower side of the magnetic field. The values of both $g_\perp$ and g_{II} are greater than the g value of free electron g_e = 2.0023. From the position of the above-mentioned g values, it can be said that Cu^{2+} is coordinated in the octahedral coordination of TiO_2 and has substituted Ti^{4+} on the lattice site [15]. The EPR peak is also broad which indicates the presence of dipolar interaction among neighboring Cu^{2+} ions that leads to the increase in the width of the EPR peak.

Study of optical properties

The diffuse reflectance spectra of pure and doped TiO_2 are shown in Figure 6a. The method adopted to acquire the absorption spectra of powder samples in DRS mode is that of Kubelka-Munk. The equation for the Kubelka-Munk method is represented by $F(R) = (1 - R)^2/2R$, where R is the reflectance and $F(R)$ is the absorbance [29]. The $F(R)$ curves of the samples are shown in Figure 6b.

Doped samples exhibit an absorption peak at 330 nm corresponding to the maximum absorption when electrons are excited from the valence to the conduction band. Doped samples show shifting in the absorption peak to the visible region. One absorption shifting occurs at just above 400 nm, and another big absorption hump appears in between 550 and 900 nm. In TiO_2, the valence band (VB) is composed of O 2*p* states, and the conduction band (CB) is composed of Ti 3*d* states [30]. The 330-nm absorption peak is due to electronic transition from O 2*p* to Ti 3*d*. Doped samples contain an extended absorption edge above 400 nm and a broad absorption peak in between 550 and 900 nm. The first absorption between 400 and 500 nm appears as a result of interfacial charge transfer from the O 2*p* valence band to the Cu(II) state attached to TiO_2 [31-37]. These Cu(II) states may be present either as Cu(II) nanoclusters or in the form of amorphous oxide phase of CuO. Li et al. [15] demonstrated that Cu(II) does not show this absorption peak if it is present as CuO, but displays this absorption when it is present as Cu(II) ions attached to TiO_2. However, Qiu et al. suggested that the absorption peak between 400 and 500 nm appears due to charge transfer from TiO_2 to CuO clusters in a system of CuO/TiO_2 nanocomposite [34]. Therefore, based on these observations, we can predict that the absorption appears due to charge transfer from O 2*p* to Cu(II) clusters or CuO amorphous phase. However, from EPR signals, it is found that copper is present as Cu(II) and is well placed in the octahedral coordination of TiO_2. Moreover, the broadening of the EPR line suggests that Cu^{2+}-Cu^{2+} dipolar interaction is taking place and that this is possible when Cu^{2+} is so closely associated possibly forming clusters. These may be nanoclusters of copper, since bulk copper clusters could have been detected in the diffraction pattern. Therefore, with the help of EPR results, we can suggest that the observed absorption band is due to charge transition from the valence band of TiO_2 to Cu(II) nanoclusters attached to TiO_2. Apart from the absorption band between 400 and 500 nm, doped samples contain another absorption hump extending from 550 to 900 nm. The second absorption band is mainly due to the *d*-*d* transition of Cu^{2+} in the crystalline environment of TiO_2 [31-37]. Cu^{2+} has a d^9 electronic configuration, and in the pure octahedral coordination, the ^2D state of Cu^{2+} is splitted into ^2E_g

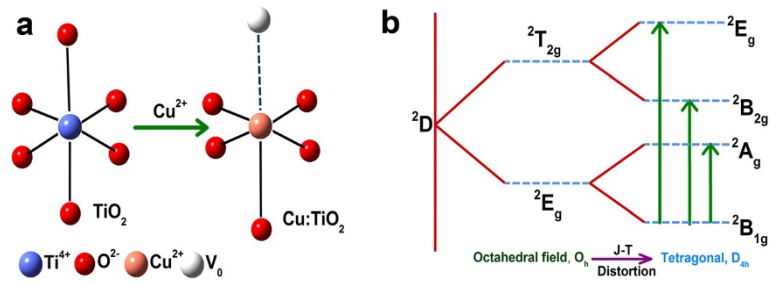

Figure 4 Distortion of the TiO_6 octahedra. (**a**) Schematic representation of the distortion of the TiO_6 octahedra on doping Cu^{2+}ion on the Ti^{4+}lattice site. Doping of Cu^{2+} on Ti^{4+} generates oxygen vacancies (white ball) nearby Cu^{2+} (shown by a dashed line). (**b**) Jahn-Teller (J-T) distortion of the octahedral symmetry of TiO_6 and changes in the *d*-*d* transition from octahedral to tetragonal. In undistorted octahedral coordination, only a single electronic transition occurs. On the other hand, due to the J-T effect, three possible *d*-*d* excitations may occur.

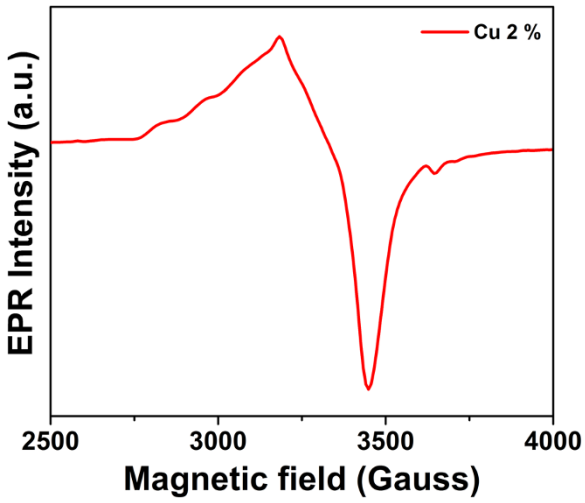

Figure 5 Room-temperature EPR spectra of 2% Cu-doped TiO_2 nanoparticles.

ground state and $^2T_{2g}$ excited state with a single electronic transition. However, from the XRD and Raman spectra of the samples, it was found that doping of Cu^{2+} generates oxygen vacancies which lie near Cu^{2+}. Therefore, Cu^{2+} is no longer in the pure octahedral (O_h) symmetry, and the symmetry is slightly distorted. A Jahn-Teller (J-T) distortion is taking place, changing the symmetry from O_h to D_{4h} [35]. Due to the J-T effect, the ground state ^2E_g is further splitted into $^2B_{1g}$ ground and ^2A_g excited states, and the $^2T_{2g}$ is separated into $^2B_{2g}$ ground and ^2E_g excited states [35,36]. Therefore, the possible optical transitions that may give rise to the above peaks are $^2B_{1g} \rightarrow {}^2A_g$, $^2B_{1g} \rightarrow {}^2B_{2g}$, and $^2B_{1g} \rightarrow {}^2E_g$. In reports, the absorption at 450 and 900 nm and the broad band at 810 nm are assigned to $^2B_{1g}$ to ^2E_g and $^2B_{1g}$ to $^2B_{2g}$ transitions, respectively [35-38]. This absorption peak cannot be shown by Cu^+, since Cu^+ has completely filled $3d^{10}$ configurations. Since $3d^{10}$ is highly stable, photoexcitation will not release electrons, and therefore, no absorption will appear. The *d-d* electronic transition of Cu^{2+} is shown in Figure 4b.

From the absorption spectra of the samples, it is understood that doping shifts the absorption edge of TiO_2 from the UV to visible region. Now, we can determine the effective reduction in the band gap (BG) of TiO_2 due to the incorporation of Cu^{2+} ions. Figure 6c shows the band gap of all samples. For BG determination, $[F(R)h\nu]^n$ is plotted against $h\nu$. Since anatase TiO_2 is an indirect band gap semiconductor, the value of n = ½ (n = 2 for direct band gap) [29]. The line drawn on the linear part of $[F(R)h\nu]^{1/2}$ vs. $h\nu$ curve at $[F(R)h\nu]^{1/2} = 0$ gives the band gap. From UV–vis spectroscopy, it is found that Cu^{2+} forms sub-band states in the band gap of TiO_2 [39]. Along with Cu^{2+}, oxygen defect band states are also formed in the band gap. In pure TiO_2, the electronic transition occurs directly from VB to CB. However, on Cu doping, the electrons are not directly excited to CB since the unoccupied Cu^{2+}*s-d* states and oxygen vacancies capture the electrons. The charged oxygen defect states formed in TiO_2 are F (two electrons), F^+ (single electron), and F^{++} (devoid of electrons) [40]. The oxygen vacancy states that may capture electrons are F^+ and F^{++}, respectively. Therefore, the sub-band states of Cu^{2+} and oxygen defects are responsible for the reduction of effective band gap of TiO_2 nanoparticles. Sahu et al. [3] examined the red shift in the band gap of TiO_2 on Cu doping and examined that absorption edge shifting and band gap reduction are controlled by the surface of the nanoparticles, lattice strain, and vacancies.

We can determine the width of the defect bands formed as an intermediate state in the band gap of TiO_2. These defect band states create a band tail extending from the lower of conduction band to deep down of band gap, and similarly, the defect states very near to the valence

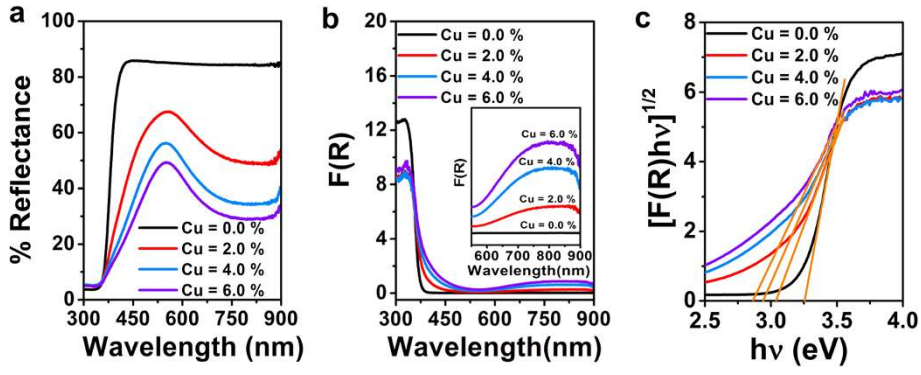

Figure 6 Diffuse reflectance, Kubelka-Munk curves, and band gap determination. (**a**) Diffuse reflectance (%*R*) spectra of pure and Cu-doped TiO_2 nanoparticles with corresponding (**b**) Kubelka-Munk absorption curves. (**c**) Determination of band gap of each samples by drawing a line at $[F(R)h\nu]^{1/2} = 0$.

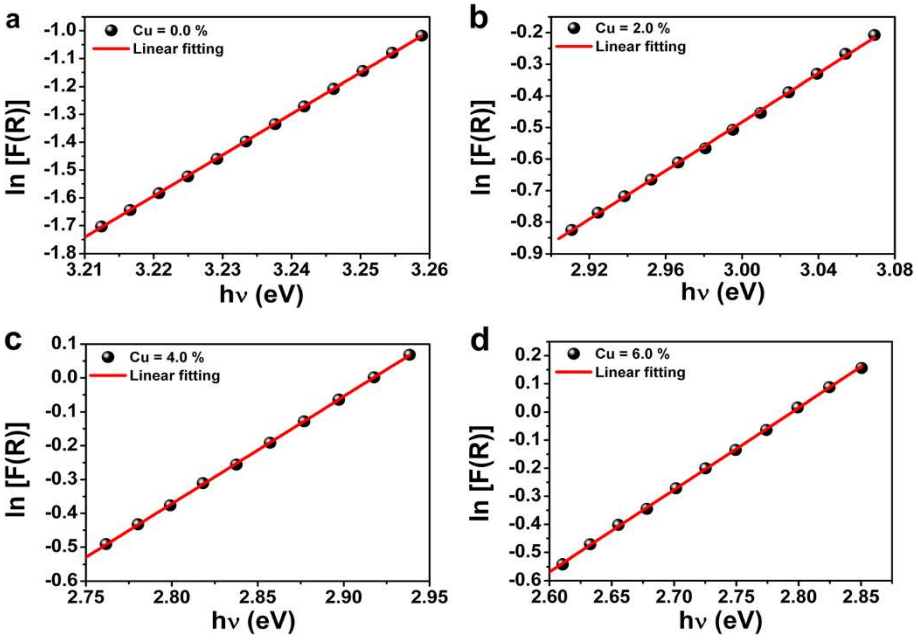

Figure 7 Plot of ln [*F*(*R*)] vs. *hυ* for the determination of Urbach energy (E_u). (**a**) 0.0%, (**b**) 2.0%, (**c**) 4.0%, and (**d**) 6.0% Cu-doped TiO_2 nanoparticles. The reciprocal of the slope of the linear fitting gives the value of E_u.

band also smear the valence band edge deep inside the gap. Therefore, on both sides of the valence band maximum and conduction band minimum, an energy tail is formed. This defect tail is known as the Urbach tail, and the energy associated with this defect tail is referred to as Urbach energy. The equation for Urbach energy is given by $\alpha = \alpha_0 \exp\left(\frac{E}{Eu}\right)$, where α is the absorption coefficient, E is the photon energy, and E_u is the Urbach energy [41,42]. The Urbach energy is calculated by plotting lnα vs. E. The reciprocal of the slopes of the linear portion, below the optical band gap, gives the value of E_u. The Urbach energy of each sample is shown in Figure 7.

Absorbance coefficient α is proportional to $F(R)$; hence, we can write ln$[F(R)]$ vs. E. The Urbach energy of pure and 2%, 4%, and 6% Cu is 67, 259, 316, and 343 meV, respectively. Therefore, as band gap decreases, the magnitude of defect energy increases. This clearly supports our argument that sub-band states formed in between the valence and conduction bands result in the narrowing of the band gap. With doping level, the number of defect levels below the conduction band increases to such an extent that the band edge is shifted deep into the forbidden gap, thereby reducing the effective band gap of TiO_2. The schematic of the formation of the Urbach tail and the relationship of the band gap with Urbach energy for different samples are shown in Figure 8a,b.

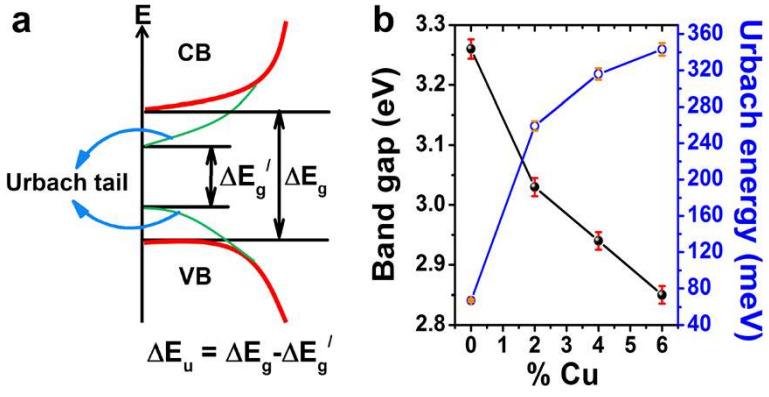

Figure 8 Result of doping and variation of the band gap. (**a**) Doping induced smearing of the valence and conduction band edges and formation of Urbach tail in Cu-doped TiO_2 nanoparticles. (**b**) Variation of band gap and Urbach energy for different concentrations of Cu.

Conclusion

Doping of Cu introduces structural defects and increases the fraction of brookite phase. The diffraction peaks are broad in the doped samples, indicating reduction in the grain size and increase in the amount of amorphous grain boundary. The small crystallite size and oxygen defects are responsible for the broadening and shifting of Raman peaks. Cu^{2+} introduces *d* states in the mid-band gap of TiO_2. The single electron in the *d* orbital undergoes Jahn-Teller distortion and gives rise to a broad absorption peak in the visible region. The *d* states of Cu^{2+} and oxygen defects are responsible for the narrowing of the band gap of TiO_2. These defects increase the magnitude of Urbach energy, and the magnitude of this energy increases as Cu loading increases.

Competing interests

The authors declare that they have no competing interests.

Authors' contributions

BC designed the objective of the work described in the text and drafted the manuscript. MD did the synthesis and performed the instrumental analysis. AC participated in the design of the study and approved the final draft of the manuscript. All authors read and approved the final manuscript.

Acknowledgments

We acknowledge the financial support provided by the Department of Science and Technology (DST), India to the project SR/NM/NS-98/2010 (G).

Received: 3 January 2013 Accepted: 27 March 2013
Published: 19 April 2013

References

1. Hashimoto, K, Irie, H, Fujishima, A: TiO_2 photocatalysis: a historical overview and future prospects. Jpn. J. Appl. Phys. **44**, 8269–8285 (2005)
2. Ni, Y, Zhu, Y, Ma, X: A simple solution combustion route for the preparation of metal-doped TiO_2 nanoparticles and their photocatalytic degradation properties. Dalton Trans. **40**, 3689–3694 (2011)
3. Sahu, M, Biswas, P: Single-step processing of copper-doped titania nanomaterials in a flame aerosol reactor. Nanoscale Res Lett. **6**, 441 (2011)
4. Xiong, LB, Li, JL, Yang, B, Yu, Y: Ti^{3+} in the surface of titanium dioxide: generation, properties and photocatalytic application. J. Nanomaterials. **2012**, 1–13 (2012)
5. Liu, G, Yang, HG, Wang, X, Cheng, L, Lu, H, Wang, L, Lu, GQ, Cheng, HM: Enhanced photoactivity of oxygen deficient anatase TiO2 with dominant 001 facets. J. Phys. Chem. C. **113**, 21784–21788 (2009)
6. Pal, M, Pal, U, Jimenez, J, Rodriguez, F: Effect of crystallization and dopant concentration on the emission behaviour of TiO_2:Eu nanophosphors. Nanoscale Res Lett. **7**, 1–12 (2012)
7. Meng, F, Hong, Z, Amdt, J, Li, M, Zhi, M, Yang, F: Visible light photocatalytic activity of nitrogen-doped $La_2Ti_2O_7$ nanosheets originating from band gap narrowing. Nano Research **5**, 213–221 (2012)
8. Cheng, C, Sun, Y: Carbon doped TiO_2 nanowire arrays with improved photoelectrochemical water splitting performance. Appl. Surf. Sci. **263**, 273–276 (2012)
9. Meng, F, Li, J, Hong, Z, Zhi, M, Sakla, A, Xiang, C, Wu, N: Photocatalytic generation of hydrogen with visible-light nitrogen-doped lanthanum titanium oxides. Catalysis Today. **199**, 48–52 (2013)
10. Choi, W, Termin, A, Hoffman, MR: The role of metal ion dopants in quantum sized TiO_2: correlation between photoreactivity and charge carrier recombination dynamics. J. Phys. Chem. **98**, 13669–13679 (1994)
11. Jaimy, BK, Safeena, VP, Ghosh, S, Hebalkar, NY, Warrier, KGK: Photocatalytic activity enhancement in doped titanium dioxide by crystal defects. Dalton Trans. **41**, 4824–4832 (2012)
12. Cao, FF, Xin, S, Guo, YG, Wan, LJ: Wet chemical synthesis of Cu/TiO_2 nanocomposites with integrated nano-current-collectors as high-rate anode materials in lithium-ion batteries. Phys. Chem. Chem. Phys. **13**, 2014–2020 (2011)
13. Arana, J, Rodriguez, JMD, Melian, JAH, Rendon, ET, Diaz, OG: Role of Pd and Cu in gas phase alcohols photocatalytic degradation with doped TiO_2. J. Photochem. Photobiol. A. **174**, 7–14 (2005)
14. Manivel, A, Naveenraj, S, Kumar, S, Selvam, P, Anandan, S: CuO-TiO_2 nanocatalyst for photodegradation of acid red 88 in aqueous solution. Sci. Adv. Mater. **2**, 51–57 (2010)
15. Li, G, Dimitrijevic, NM, Chen, L, Rajh, T: Role of surface/interfacial Cu^{2+}sites in the photocatalytic activity of coupled CuO-TiO_2 nanocomposites. J. Phys. Chem. C. **112**, 19040–19044 (2008)
16. Wang, RSH, Feng, J, Hu, X, Lock, PY: Discoloration and mineralization of non-biodegradable Azo dye orange II by copper-doped TiO_2 nanocatalysts. J. Environ. Sci. Health, Part A: Toxic/Hazard. Subst. Environ. Eng **39**, 2583–2595 (2004)
17. Wang, B, Zhao, YD, Hu, L, Cao, JS, Gao, FL, Liu, Y, Wang, LJ: Improved and excellent CO sensing properties of Cu-doped TiO_2 nanofibers. Chinese Science Bulletin **55**, 228–232 (2010)
18. Nian, JN, Chen, SA, Tsai, CC, Teng, H: Structural feature and catalytic performance of Cu species distributed over TiO_2 nanotubes. J. Phys. Chem. B. **110**, 25817–25824 (2006)
19. Slamet, Nasution, HW, Purnama, E, Kosela, S, Gunlazuardi, J: Photocatalytic reduction of CO_2 on copper-doped titania catalysts prepared by improved-impregnation method. Catal. Commun. **6**, 313–319 (2005)
20. Baghriche, O, Rtimi, S, Pulgarin, C, Sanjines, R, Kiwi, J: Effect of the spectral properties of TiO_2, Cu, TiO_2/Cu sputtered films on the bacterial inactivation under low intensity actinic light. J. Photochem. Photobiol., A **251**, 50–56 (2013)
21. So, WW, Park, SB, Kim, KJ, Shin, CH, Moon, SJ: The crystalline phase stability of titania particles prepared at room temperature by the sol–gel method. J. Mater. Sci. **36**, 4299–4305 (2001)
22. Zhang, WF, He, YL, Zhang, MS, Yin, Z, Chen, Q: Raman scattering study of anatase TiO_2 nanocrystals. J. Phys. D: Appl. Phys. **33**, 912–916 (2000)
23. Choudhury, B, Choudhury, A: Dopant induced changes in structural and optical properties of Cr doped TiO_2 nanoparticles. Mater. Chem. Phys. **132**, 1112–1118 (2012)
24. Tian, F, Zhang, Y, Zhang, J, Pan, C: Raman spectroscopy: a new approach to measure the percentage of anatase TiO_2 exposed (001) facets. J. Phys. Chem. C. **116**, 7515–7519 (2012)
25. Duhalde, S, Vignolo, MF, Golmar, F, Chiliotte, C, Rodriguez, CE, Errico, LA, Cabrera, AF, Renteria, M, Sanchez, FH, Weissmann, M: Appearance of room-temperature ferromagnetism in Cu-doped $TiO_{2-\delta}$ films. Phys. Rev. B **72**(R), 161313 (2005)
26. Parker, JC, Siegel, RW: Calibration of the Raman spectrum to the oxygen stoichiometry of nanophase TiO_2. Appl. Phys. Lett. **57**, 943–945 (1990)
27. Xue, X, Ji, W, Mao, Z, Mao, H, Wang, Y, Wang, X, Ruan, W, Zhao, B, Lombardi, JR: Raman investigation of nanosized TiO_2: effect of crystallite size and phonon confinement. J. Phys. Chem. C. **116**, 8792–8797 (2012)
28. Baltazar, P, Lara, V, Cordoba, G, Arroyo, R: Kinetics of the amorphous anatase phase transformation copper doped titanium dioxide. J. Sol–gel Sci Tech **37**, 129–133 (2006)
29. Choudhury, B, Borah, B, Choudhury, A: Ce-Nd codoping effect on the structural and optical properties of TiO_2 nanoparticles. Mater. Sci. Eng B **178**, 239–247 (2013)
30. Nagao, Y, Yoshikawa, A, Koumot, K, Kato, T, Ikuhara, Y, Ohta, H: Experimental characterization of the electronic structure of anatase TiO_2: thermopower modulation. Appl. Phys. Lett. **97**, 172112 (2010)
31. Komova, OV, Simakov, AV, Rogov, VA, Kochubei, DI, Odegova, GV, Kriventsov, VV, Puakshitis, EA, Ushakov, VA, Sazonova, NN, Nikoro, TA: Investigation of the state of copper in supported copper-titania oxide catalysts. J. Mol. Catal. A: Chem. **161**, 191–204 (2000)
32. Liu, M, Qiu, X, Miyauchi, M, Hashimoto, K: Cu(II) oxide amorphous nanoclusters grafted Ti^{3+} self-doped TiO_2: an efficient visible light photocatalyst. Chem. Mater. **23**, 5582–5586 (2011)
33. Irie, H, Miura, S, Kamiya, K, Hashimoto, K: Efficient visible light sensitive photocatalysts: grafting of Cu (II) ion onto TiO_2 and WO_3 photocatalysts. Chem Phys Lett **457**, 202–205 (2008)
34. Qiu, X, Miyauchi, M, Sunada, K, Minoshima, M, Liu, M, Lu, Y, Li, D, Shimodaira, Y, Hosogi, Y, Kuroda, Y, Hashimoto, K: Hybrid Cu_xO/TiO_2 nanocomposite as risk reduction materials in indoor environments. ACS Nano **6**, 1609–1618 (2012)
35. Ramadevudu, G, Shareefuddin, N, Bai, S, Rao, ML, Chary, MN: Electron paramagnetic resonance and optical absorption studies of Cu^{2+} spin probe in MgO-Na_2O-B_2O_3 ternary glasses. J. Non-Cryst. Solids **278**, 205–212 (2000)

36. Somasekharam, V, Siva Prasad, P, Ramesh, K, Reddy, YP: Electronic spectra of VO^{2+} and Cu^{2+} ions in rubidium zinc sulphate hexahydrate. Physica Scripta. **33**, 169–172 (1986)
37. Kamalaker, V, Upender, G, Prasad, M, Mouli, VC: Infrared, ESR and optical absorption studies of Cu^{2+} ions doped in TeO_2-ZnO-NaF glass system. Indian J. Pure Appl. Phys. **48**, 709–715 (2010)
38. Chakradhar, S, Ramesh, KP, Rao, JL, Ramakrishna, J: Mixed alkali effect in borate glasses-electron paramagnetic resonance and optical absorption studies in Cu^{2+} doped xNa_2O-(3-x) K_2O-$70B_2O_3$ glasses. J. Phys. Condens. Matter. **15**, 1469 (2003)
39. Lalitha, K, Sadanandam, G, Kumari, VD, Subrahmanyam, M, Sreedhar, B, Hebalkar, NY: Highly stabilized and finely dispersed Cu_2O/TiO_2: a promising visible sensitive photocatalyst for continuous production of hydrogen from glycerol: water mixtures. J. Phys. Chem. C. **114**, 22181–22189 (2010)
40. Serpone, N: Is the band gap of pristine TiO_2 narrowed by anion and cation doping of titanium dioxide in second generation photocatalysts? J. Phys. Chem. B. **110**, 24287–24293 (2006)
41. Boubaker, K: A physical explanation to the controversial Urbach tailing universality. Eur. Phys. J. Plus **126**, 10 (2011)
42. Choudhury, B, Borah, B, Choudhury, A: Extending photocatalytic activity of TiO_2 nanoparticles to visible region of illumination by doping of cerium. Photochem. Photobiol. **88**, 257–264 (2012)

doi:10.1186/2228-5326-3-25
Cite this article as: Choudhury *et al.*: **Defect generation, *d-d* transition, and band gap reduction in Cu-doped TiO_2 nanoparticles.** *International Nano Letters* 2013 **3**:25.